



ORIGINAL CLINICAL SCIENCE

Clinical and functional relevance of right ventricular contraction patterns in pulmonary hypertension

Zvonimir A. Rako, MD,^{a,1} Athiththan Yogeswaran, MD,^{a,1}
 Bálint K. Lakatos, MD,^b Alexandra Fábíán, MD,^b Selin Yildiz,^a
 Bruno Brito da Rocha,^a István Vadász, MD, PhD,^a
 Hossein Ardeschir Ghofrani, MD,^{a,c,d} Werner Seeger, MD,^a
 Henning Gall, MD, PhD,^a Nils C. Kremer, MD,^a Manuel J. Richter, MD,^a
 Pascal Bauer, MD,^e Ryan J. Tedford, MD,^f Robert Naeije, MD, PhD,^g
 Attila Kovács, MD, PhD,^{b,1} and Khodr Tello, MD^{a,1}

From the ^aDepartment of Internal Medicine, Justus-Liebig-University Giessen, Universities of Giessen and Marburg Lung Center (UGMLC), Member of the German Center for Lung Research (DZL), Giessen, Germany; ^bHeart and Vascular Center, Semmelweis University, Hungary; ^cDepartment of Pneumology, Kerckhoff Heart, Rheuma and Thoracic Center, Bad Nauheim, Germany; ^dDepartment of Medicine, Imperial College London, London, UK; ^eDepartment of Cardiology & Angiology, University of Giessen, Giessen, Germany; ^fDepartment of Medicine, Division of Cardiology, Medical University of South Carolina, Charleston, South Carolina; and the ^gFree University of Brussels, Brussels, Belgium.

KEYWORDS:

pulmonary
hypertension;
pulmonary arterial

BACKGROUND: The right ventricle has a complex contraction pattern of uncertain clinical relevance. We aimed to assess the relationship between right ventricular (RV) contraction pattern and RV-pulmonary arterial (PA) coupling defined by the gold-standard pressure–volume loop-derived ratio of end-systolic/arterial elastance (Ees/Ea).

Abbreviations: 2D, two-dimensional; 3D, three-dimensional; 4CH, four-chamber; 4F/8F, 4 French/8 French (measure for catheter size); α , fitting constant; AEF, anteroposterior ejection fraction; AUC, area under the curve; β , end-diastolic stiffness; BD, beginning of diastole; BSA, body surface area; CO, cardiac output; Ea, arterial elastance; ED, end of diastole; EDP, end-diastolic pressure; EDPVR, end-diastolic pressure–volume relationship; EDV, end-diastolic volume; Eed, end-diastolic elastance; Ees, end-systolic elastance; EF, ejection fraction; ERS, European Respiratory Society; ESC, European Society of Cardiology; ESP, end-systolic pressure; ESPVR, end-systolic pressure–volume relationship; ESV, end-systolic volume; HFpEF, heart failure with preserved ejection fraction; LEF, longitudinal ejection fraction; LV, left ventricular; LVEF, left ventricular ejection fraction; LVSVi, left ventricular stroke volume indexed to body surface area; mPAP, mean pulmonary arterial pressure; PA, pulmonary arterial; PAH, pulmonary arterial hypertension; PASP, pulmonary arterial systolic pressure; PAWP, pulmonary arterial wedge pressure; PH, pulmonary hypertension; PV, pressure–volume; PVR, pulmonary vascular resistance; REF, radial ejection fraction; RV, right ventricular; RVEDA, right ventricular end-diastolic area; RVEDV, right ventricular end-diastolic volume; RVEDVi, right ventricular end-diastolic volume indexed to body surface area; RVEF, right ventricular ejection fraction; RVESA, right ventricular end-systolic area; RVESV, right ventricular end-systolic volume; RVESVi, right ventricular end-systolic volume indexed to body surface area; RVFAC, right ventricular fractional area change; RVFWLS, right ventricular free wall longitudinal strain; RVGLS, right ventricular global longitudinal strain; RVIT, right ventricular inflow tract; RVOT, right ventricular outflow tract; RVSV, right ventricular stroke volume; RVSVi, right ventricular stroke volume indexed to body surface area; S', peak systolic velocity of the lateral tricuspid insertion; SV, stroke volume; SVi, stroke volume index; SvO₂, mixed venous oxygen saturation; TAPSE, tricuspid annular plane systolic excursion; WHO, World Health Organization; V, volume

Reprint requests: Khodr Tello, MD, Department of Internal Medicine, Justus Liebig University Giessen, Universities of Giessen and Marburg Lung Center (UGMLC), German Center for Lung Research (DZL), Klinikstrasse 33, 35392 Giessen, Germany.

E-mail address: khodr.tello@innere.med.uni-giessen.de.

¹ These authors have contributed equally to this work.

hypertension;
heart failure with
preserved ejection
fraction;
right ventricular
contraction pattern;
three-dimensional
echocardiography;
right ventricular-
pulmonary arterial
coupling

METHODS: Prospectively enrolled patients with suspected or confirmed pulmonary hypertension underwent three-dimensional echocardiography, standard right heart catheterization, and RV conductance catheterization. RV–PA uncoupling was categorized as severe ($Ees/Ea < 0.8$), moderate ($Ees/Ea 0.8-1.29$), and none/mild ($Ees/Ea \geq 1.3$). Clinical severity was determined from hemodynamics using a truncated version of the 2022 European Society of Cardiology/European Respiratory Society risk stratification scheme.

RESULTS: Fifty-three patients were included, 23 with no/mild, 24 with moderate, and 6 with severe uncoupling. Longitudinal shortening was decreased in patients with moderate vs no/mild uncoupling ($p < 0.001$) and intermediate vs low hemodynamic risk ($p < 0.001$), discriminating low risk from intermediate/high risk with an optimal threshold of 18% (sensitivity 80%, specificity 87%). Anteroposterior shortening was impaired in patients with severe vs moderate uncoupling ($p = 0.033$), low vs intermediate risk ($p = 0.018$), and high vs intermediate risk ($p = 0.010$), discriminating high risk from intermediate/low risk with an optimal threshold of 15% (sensitivity 100%, specificity 83%). Left ventricular (LV) end-diastolic volume was decreased in patients with severe uncoupling ($p = 0.035$ vs no/mild uncoupling).

CONCLUSIONS: Early RV–PA uncoupling is associated with reduced longitudinal function, whereas advanced RV–PA uncoupling is associated with reduced anteroposterior movement and LV preload, all in a risk-related fashion.

CLINICALTRIALS.GOV: NCT04663217

J Heart Lung Transplant xxx;xxx:xxx-xxx

© 2023 International Society for Heart and Lung Transplantation. All rights reserved.

Right ventricular (RV) functional adaptation to afterload is a major determinant of symptomatology and outcome in severe pulmonary hypertension (PH).^{1,2} Progression of PH is initially associated with increased RV contractility to preserve RV–pulmonary arterial (PA) coupling until this homeometric mechanism is exhausted, resulting in a heterometric increase in dimensions, systemic congestion, and eventual impairment of left ventricular (LV) filling.^{1,2} The system has reserve, as it has been shown that RV–PA coupling (measured as the end-systolic/arterial elastance ratio [Ees/Ea]) has to decrease by approximately half before RV end-systolic and end-diastolic volumes (RVESV and RVEDV, respectively) become higher than normal.³

RV contraction is a complex peristaltic phenomenon, with longitudinal shortening generally thought to be the major determinant of ejection.² This concept is derived from two-dimensional (2D) echocardiographic studies in healthy individuals and in patients with pulmonary arterial hypertension (PAH).⁴ However, magnetic resonance imaging studies showed an important contribution of transverse shortening, particularly in advanced PAH.^{5,6} This may explain why RV longitudinal shortening (assessed as tricuspid annular plane systolic excursion [TAPSE]) was found to be related to systolic function (assessed as cardiac index), while transverse shortening was instead found to be related to PA pressure.⁷ Three-dimensional (3D) echocardiography has demonstrated that all strain vectors may be reduced in patients with PH, but with longitudinal strain showing a lesser correlation than circumferential strain with RV ejection fraction (RVEF).⁸

This study used 3D echocardiography and invasive measurements of RV–PA coupling to investigate whether contraction patterns are associated with RV functional adaptation to afterload and mortality risk in patients with PH of various causes and severities. The results suggest that

RV contraction patterns may be functionally and clinically relevant.

Methods

Study population and study design

This study is a posthoc and exploratory analysis of data from the prospectively recruiting EXERTION study (ClinicalTrials.gov Identifier: NCT04663217). The EXERTION study was in accordance with the principles of the Declaration of Helsinki and was approved by the local Ethics Committee of the Faculty of Medicine at the University of Giessen (Az: 117/16). All patients gave written informed consent. All authors had access to the entire data record included in this study and take responsibility for its integrity and analysis.

The inclusion and exclusion criteria for the EXERTION study are outlined in [Table S1](#). For the current analysis, patients with atrial fibrillation were excluded because of impaired comparability of cardiac cycles due to altering cycle length. The patients either received initial invasive diagnostic evaluation for suspected PH or were enrolled in the course of a known PH diagnosis. PH was diagnosed in accordance with current guidelines.⁹ The diagnoses were made by a multidisciplinary board comprising pneumologists and radiologists. If PH was excluded at the initial invasive diagnostic evaluation, the patient was classed as a control. All patients underwent echocardiography, including 3D and strain echocardiography, as well as right heart catheterization with a fluid-filled balloon-tipped thermodilution catheter and a conductance catheter to measure RV pressures and volumes ([Figure 1A, B](#)).

The interval between echocardiography and right heart catheterization was mainly 1 day (4 patients received echocardiography within 3 days of right heart catheterization, and 2 patients within 5 days). In each case, no adjustment of relevant medication, especially PH-specific medication and diuretics, was performed during the interval between echocardiography and right heart catheterization.

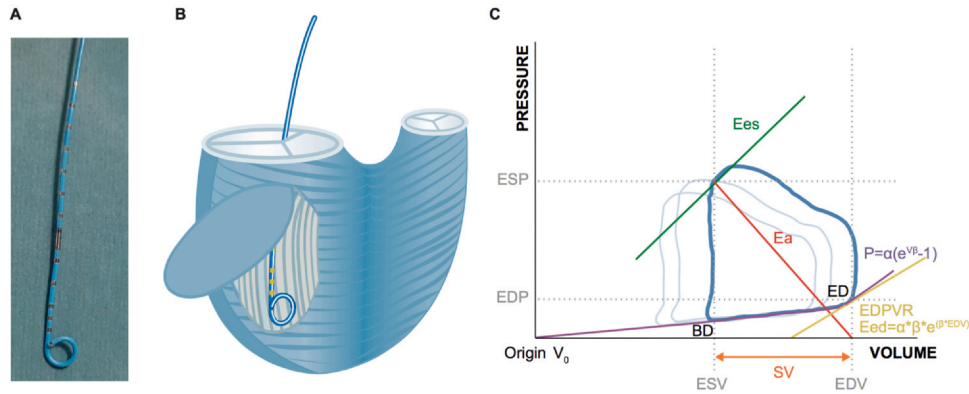


Figure 1 Conductance catheterization of the right ventricle. (A) A conductance catheter. The electrodes generate a segmented electric field within the RV lumen. Conductivity alters with RV volume alteration, and volume can be derived in real-time. Pressure is measured simultaneously, allowing generation of pressure-volume loops. (B) Model of the RV myocardium with a correctly positioned conductance catheter (apical pigtail and all electrodes within the right ventricle). Subendocardial myofibers are longitudinally orientated, whereas subepicardial myofibers run radially. (C) Pressure–volume loop schematic showing derived parameters. α , curve fit parameter; β , end-diastolic stiffness; BD, beginning of diastole; Ea, arterial elastance; ED, end of diastole; EDP, end-diastolic pressure; EDPVR, end-diastolic pressure–volume relationship; EDV, end-diastolic volume; Eed, end-diastolic elastance; Ees, end-systolic elastance; ESP, end-systolic pressure; ESV, end-systolic volume; P, pressure; RV, right ventricular; SV, stroke volume; V, volume; V₀, pressure-released volume.

Echocardiography

Echocardiography was performed with the Philips EPIQ 7G ultrasonic unit (Philips Healthcare, the Netherlands), using the X5-1 ultrasound probe, according to current guidelines.¹⁰ Patients were examined in a left lateral lying position. Standardized acquisition of optimally adjusted RV-focused apical 4-chamber (4CH) views was conducted to capture the entire RV endocardium for analysis, and 3D data sets were recorded applying the “HM ACQ” tool. Images were exported to the Philips IntelliSpace Cardiovascular workstation (Koninklijke Philips N.V., the Netherlands) for external analysis. “4D RV-FUNCTION 2” software (TomTec Imaging GmbH, Unterschleissheim, Germany) was applied for volumetric reanalysis and export of 3D RV beutel data sets for ReVISION analysis.¹¹ Endocardial borders of the cardiac chambers were automatically tracked by 3D speckle tracking, with the examiner being able to perform manual adjustments subsequently. For LV volumetry, “DHM” software (Dynamic HeartModel^{A.1.}, Philips Healthcare) and “4D LV-ANALYSIS 3” software (TomTec Imaging GmbH) were used. Furthermore, 2D echocardiographic parameters were acquired. TAPSE was obtained in M-mode by adjusting to the lateral insertion of the tricuspid valve into the basal RV free wall. Peak systolic velocity of the lateral tricuspid insertion (S') was obtained from tissue Doppler imaging and pulsed-wave Doppler at the basal compartment of the RV free wall. Planimetric measurement of RV end-diastolic area (RVEDA) and RV end-systolic area (RVESA) was performed in the right ventricle-focused 4CH view. RV fractional area change (RVFAC) was calculated as (RVEDA – RVESA)/RVEDA. RV free wall longitudinal strain (RVFWLS) and RV global longitudinal strain (RVGLS) were determined using the option “AutoStrain RV” (Koninklijke Philips N.V.).

To assess inter- and intraobserver variability of RV volumetry, 2 experienced investigators (Z.R., S.Y.) independently performed repeated measurements in a set of 15 randomly selected patients. The investigators were unaware of clinical features and diagnosis.

ReVISION analysis

ReVISION software (Argus Cognitive, Inc, Lebanon, NH) was applied for automatic isolated quantification of longitudinal (LEF),

radial (REF), and anteroposterior (AEF) ejection fraction, as published and validated previously.^{11,12} Of note, this composition of LEF, REF, and AEF is not additive; the sum does not equal total RVEF. LEF principally describes the motion of the RV base, including the tricuspid valve, toward the apex. REF describes the movement of the RV free wall toward the interventricular septum. AEF principally describes the shortening between the anterior and posterior insertion lines of the RV free wall into the interventricular septum.

Right heart catheterization

All participants underwent a standard right heart catheterization in conformance with updated guidelines⁹ to measure mean PA pressure (mPAP), central venous pressure, RV pressure, and PA wedge pressure (PAWP). Cardiac output (CO) was measured by the (in-) direct Fick method in all patients (35 patients [66%] with the direct Fick method). Cardiac index was defined as the ratio of CO and calculated body surface area (BSA). BSA was determined as described by DuBois (BSA = 0.007184 * height^{0.725} * weight^{0.425}). Pulmonary vascular resistance (PVR) was calculated as PVR = (mPAP – PAWP)/CO.

RV conductance catheterization

A 4F conductance catheter (CA-No. 41063, CD Leycom, Zoetermeer, the Netherlands, see Figure 1A) was inserted into the internal jugular vein via an 8F introducer sheath. The catheter was positioned within the right ventricle with the catheter tip reaching apically under echocardiographic guidance and supervision of pressure–volume (PV) loops, which were simultaneously obtained by the intracardiac analyzer (Inca, CD Leycom). PV loops were displayed on-screen in real-time for consecutive cardiac cycles and were calibrated to resting volumetry derived from 3D echocardiography. The multibeat method was applied to determine Ees and Ea. As previously described,¹³ sequential resting PV loops were initially recorded. The Valsalva maneuver was then executed for preload reduction, resulting in a stepwise leftward shift of end-systolic PV points of consecutive loops, which were concatenated by a regression line representing the end-systolic PV relationship

(ESPVR). The intersection of the ESPVR and the x axis determined V_0 (Figure 1C), which theoretically represents the unstressed RV volume. A line was constructed connecting V_0 and the end-systolic PV coordinate of a resting PV loop, and Ees was determined as the slope of that line. Ea was determined as the ratio of RV end-systolic pressure to stroke volume (RVSV; Figure 1C). PV loops were recorded successively and were checked for suitability. Three to 5 applicable PV loops were included for each patient, and mean values were calculated for both Ees and Ea. End-diastolic elastance (Eed) was calculated as the end-diastolic PV relationship ($dP/dV = \alpha\beta * e^{\beta * EDV}$; see Figure 1C) averaged on 3 PV loops.

Stratification by RV–PA coupling

The study population was divided into 3 groups according to RV–PA coupling. Severe RV–PA uncoupling was defined as Ees/Ea < 0.8.³ Near-normal and intermediate RV–PA uncoupling were defined based on the median Ees/Ea value in the remaining patients: Ees/Ea below the median value was classed as intermediate uncoupling and Ees/Ea equal to or greater than the median value was classed as no or mild uncoupling.

Hemodynamic risk stratification

Risk assessment was performed in keeping with the current European Society of Cardiology/European Respiratory Society (ESC/ERS) guidelines.⁹ A truncated version of the ESC/ERS risk stratification scheme including cardiac index, indexed SV (SV_i), central venous pressure, and mixed venous oxygen saturation was applied. Each hemodynamic variable was graded in a 3-strata model where 1 = “Low risk,” 2 = “Intermediate risk,” and 3 = “High risk.” Dividing the sum of all grades by the number of available variables for each patient rendered a mean grade. The mean grade was rounded off to the nearest integer, which was used to define the patient’s hemodynamic risk group, as previously reported.¹⁴

Statistical analysis

The Shapiro-Wilk test for normality was applied for each included parameter, with $p \geq 0.05$ indicating normal distribution. Normally distributed data are presented as mean \pm standard deviation. Non-normally distributed data are presented as median [interquartile range].

To assess differences between groups, we used chi-square tests for categorical data, *t*-tests for normally distributed continuous data, and Wilcoxon’s rank sum tests for continuous data with a non-normal distribution.

Receiver operating characteristic analyses were performed to assess the discriminatory power of parameters for detection of patients at high risk, as previously described.¹⁵ Each analysis was performed with R version 4.0 (The R Foundation, Vienna); 2-sided $p < 0.05$ indicated statistical significance.

Results

Characteristics of the study population

Seventy patients were enrolled between November 2020 and December 2021. Eight patients were excluded, as 3D RV beutel construction and export were not possible. Nine further patients with atrial fibrillation were excluded. Thus

Table 1 Demographic and Clinical Characteristics of the Study Population

Parameter	All participants (<i>n</i> = 53)
Age, years	68.0 [57.0, 76.0]
Sex, <i>n</i> (%)	
Male	17 (32)
Female	36 (68)
Body mass index, kg/m ²	28.4 [23.6, 33.2]
Diagnosis, <i>n</i> (%)	
Idiopathic PAH	9 (17)
PAH associated with rheumatologic disease	1 (2)
PAH associated with systemic sclerosis	1 (2)
Portopulmonary hypertension	1 (2)
Pulmonary veno-occlusive disease	1 (2)
HFpEF-PH	6 (11)
HFpEF-non-PH	3 (6)
Chronic thromboembolic PH	17 (32)
CTEPD without PH	3 (6)
Controls	11 (21)
WHO functional class, <i>n</i> (%)	
I	2 (4)
II	13 (25)
III	35 (66)
IV	3 (6)
Brain natriuretic peptide, pg/ml	62 [20,169]

Abbreviations: CTEPD, chronic thromboembolic pulmonary disease; HFpEF, heart failure with preserved ejection fraction; PAH, pulmonary arterial hypertension; PH, pulmonary hypertension; WHO, World Health Organization.

Normally distributed data are presented as mean \pm standard deviation; non-normally distributed data are presented as median [interquartile range].

53 patients were included in the study (Figure S1). The median age of the study population was 68 [57, 76] years, and 36 patients (68%) were female (Table 1). Of the included patients, 21% were in the control group whereas 32%, 17%, and 11% were diagnosed with chronic thromboembolic PH, idiopathic PAH, and PH due to heart failure with preserved EF (HFpEF), respectively. Baseline characteristics of the control patients (with invasive exclusion of PH) are shown in Table S2. The majority of the included patients showed dyspnea corresponding to World Health Organization (or New York Heart Association for the patients with HFpEF) functional class III. Further baseline characteristics including echocardiography, standard right heart catheterization, and conductance RV catheterization data are presented in Tables 1–3.

The 3D echocardiographic RV volumetry showed good inter- and intraobserver reliability. The intraclass correlation coefficient was 0.977 for RVEDV, 0.986 for RVESV, 0.966 for RVSV, and 0.976 for RVEF. The interclass correlation coefficient was 0.908 for RVEDV, 0.920 for RVESV, 0.836 for RVSV, and 0.826 for RVEF.

Six patients had severe RV–PA uncoupling (Ees/Ea < 0.8). The median Ees/Ea value in the remaining patients

Table 2 Clinical Characteristics of the Study Population—Imaging Parameters

Parameter	All participants (<i>n</i> = 53)
TAPSE, mm	20.9 ± 3.8
PASP, mm Hg ^a	50.5 [33,75]
TAPSE/PASP, mm/mm Hg ^a	0.420 [0.252, 0.700]
Right atrial end-systolic area, cm ²	16.6 [12.3, 21.7]
S', cm/s	11.0 [9.7, 12.5]
RV fractional area change, %	35.5 [25.3, 43.4]
RV global longitudinal strain, %	-18.6 ± 5.0
RV free wall longitudinal strain, %	-23.3 ± 6.3
RV end-diastolic volume, ml	123.5 ± 43.1
RV end-diastolic volume indexed to BSA, ml/m ²	64.3 ± 23.1
RV end-systolic volume, ml	63.1 [45.6, 89.8]
RV end-systolic volume indexed to BSA, ml/m ²	32.6 [23.1, 48.7]
RV stroke volume, mL	51.8 ± 15.3
RV stroke volume indexed to BSA, ml/m ²	26.8 ± 6.9
RV ejection fraction, %	45.1 [36.9, 51.8]
LV end-diastolic volume, ml	119.2 ± 33.9
LV end-diastolic volume indexed to BSA, ml/m ²	61.1 ± 13.4
LV end-systolic volume, ml	48.6 ± 16.9
LV end-systolic volume indexed to BSA, ml/m ²	24.6 [19.5, 28.3]
LV stroke volume, ml	70.6 ± 19.4
LV stroke volume indexed to BSA, ml/m ²	36.3 ± 7.9
LV ejection fraction, %	59.5 ± 5.6
Longitudinal ejection fraction, %	18.1 [16.1, 22.1]
Radial ejection fraction, %	17.6 [11.1, 22.0]
Anteroposterior ejection fraction, %	20.1 [14.8, 23.8]

Abbreviations: BSA, body surface area; LV, left ventricular; PASP, pulmonary arterial systolic pressure; RV, right ventricular; S', peak systolic velocity of the lateral tricuspid insertion; TAPSE, tricuspid annular plane systolic excursion.

Normally distributed data are presented as mean ± standard deviation; non-normally distributed data are presented as median [interquartile range].

^a*n* = 46.

was 1.3; 23 patients had no or mild RV-PA uncoupling (Ees/Ea ≥ 1.3) and 24 patients had intermediate RV-PA uncoupling (Ees/Ea 0.8-1.29). Inter- and intraobserver reliability was excellent, with inter- and intraclass correlation coefficients of 0.985 and 0.999, respectively, for Ees and 0.998 and 0.997, respectively, for Ea.

Hemodynamic alterations relative to RV-PA coupling

Increasing RV-PA uncoupling was associated with hemodynamic alterations characteristic of PH; details are shown in Figure S2, and are briefly summarized here. Parameters indicating RV afterload (mPAP, PVR, and Ea) were increased with mounting RV-PA uncoupling (*p* < 0.05). RV diastolic

Table 3 Clinical Characteristics of the Study Population—Hemodynamic Parameters

Parameter	All participants (<i>n</i> = 53)
End-diastolic elastance, mm Hg/ml	0.178 [0.140, 0.267]
Ees, mm Hg/ml	0.713 ± 0.312
Ea, mm Hg/ml	0.534 [0.349, 0.864]
Ees/Ea	1.201 [0.961, 1.470]
Mean pulmonary arterial pressure, mmHg	27 [19,40]
Pulmonary arterial wedge pressure, mmHg	10 [6,11]
Central venous pressure, mmHg	6 [5,9]
Pulmonary vascular resistance, dyn·s/cm ⁵	248 [139,533]
Cardiac index, l/min/m ²	2.7 [2.2, 3.1]
Stroke volume index, ml/m ²	39.62 ± 11.07
Mixed venous oxygen saturation, %	66.6 ± 6.3

Abbreviations: Ea, arterial elastance; Ees, end-systolic elastance. Normally distributed data are presented as mean ± standard deviation; non-normally distributed data are presented as median [interquartile range].

stiffness (Eed) increased comparing severe uncoupling with no or mild uncoupling (*p* = 0.006). By contrast, RV contractility (Ees) was not increased. Cardiac index was reduced in patients with intermediate uncoupling compared with those with no or mild uncoupling (*p* = 0.007).

Analysis of RV shortening along 3 spatial axes related to RV-PA coupling

RV shortening was analyzed along 3 axes, quantifying longitudinal, radial, and anteroposterior shortening. Comparing intermediate with no or mild RV-PA uncoupling, LEF was impaired (17 [14-19] compared with 22 [19-26]%; *p* < 0.001), whereas REF (*p* = 0.18) and AEF (*p* = 0.97) were unchanged (Figure 2A). Comparing severe with intermediate RV-PA uncoupling, AEF was decreased (12 [7-15]% compared with 21 [13-25]%; *p* = 0.033), whereas REF (*p* = 0.27) and LEF (*p* = 0.49) remained unchanged. A sensitivity analysis restricted to patients with precapillary PH or chronic thromboembolic pulmonary disease and control patients (*n* = 43, Table S3) demonstrated a similar evolution of RV contraction patterns (Figure S3A).

2D echocardiographic parameters of longitudinal RV function (TAPSE, S', RVGLS, and RVFWLS) declined with decreasing Ees/Ea (Figure S4A-D). TAPSE, RVGLS, and RVFWLS revealed a longitudinal RV functional impairment between no or mild uncoupling and intermediate uncoupling (*p* = 0.041 for TAPSE, *p* = 0.022 for RVGLS, and *p* = 0.010 for RVFWLS) but not between intermediate and severe uncoupling; the decline in S' was not significant in either comparison. RVFAC (Figure S4E) was altered between no or mild uncoupling and intermediate uncoupling (*p* = 0.020), as well as between intermediate and severe uncoupling (*p* = 0.005).

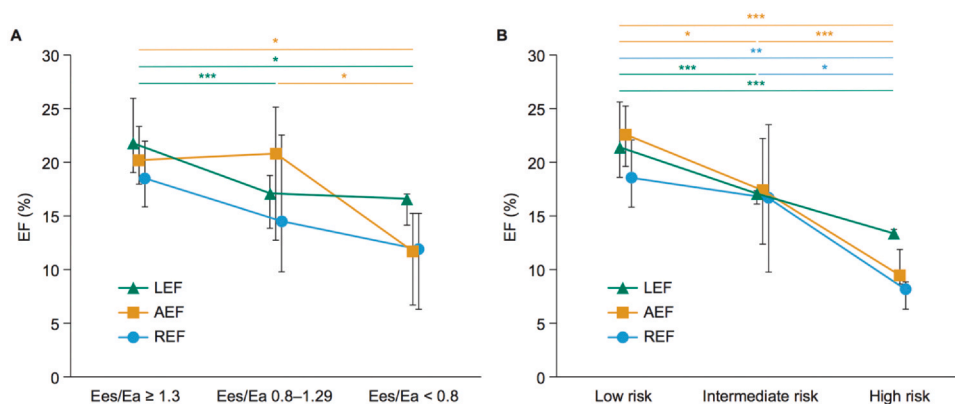


Figure 2 RV shortening in relation to RV-PA coupling and risk. LEF for longitudinal, REF for radial, and AEF for anteroposterior shortening of the right ventricle (A) in relation to RV-PA coupling as indicated by Ees/Ea (no or mild uncoupling: Ees/Ea ≥ 1.3 [$n = 23$]; intermediate uncoupling: Ees/Ea 0.8–1.29 [$n = 24$]; severe uncoupling: Ees/Ea < 0.8 [$n = 6$]) and (B) in relation to simplified hemodynamic-based risk stratification according to European Society of Cardiology/European Respiratory Society guidelines (low hemodynamic risk: $n = 30$; intermediate hemodynamic risk: $n = 17$, high hemodynamic risk: $n = 6$).⁹ Medians and interquartile ranges are shown. * $p < 0.05$; ** $p < 0.01$; *** $p < 0.001$. AEF, anteroposterior ejection fraction; Ea, arterial elastance; Ees, end-systolic elastance; EF, ejection fraction; LEF, longitudinal ejection fraction; PA, pulmonary arterial; REF, radial ejection fraction; RV, right ventricular.

Hemodynamic-based risk stratification

Comparing intermediate ($n = 17$) with low hemodynamic risk ($n = 30$), a loss of longitudinal and anteroposterior shortening was noted (LEF: 17.1 [16.1–17.4]% vs 21.4 [18.6–25.7]%, $p < 0.001$; AEF: 17.4 [12.4–22.3]% vs 22.6 [19.7–25.3]%, $p = 0.018$; Figure 2B). A sensitivity analysis restricted to patients with precapillary PH or chronic thromboembolic pulmonary disease and control patients demonstrated similar behavior of RV contraction patterns in relation to hemodynamic risk (Figure S3B). LEF showed good discriminatory power between low and intermediate/high hemodynamic risk which was exceeded by TAPSE/PASP, whereas REF and AEF had lower discriminatory power (Figure 3A–D). The optimal cut-off to discriminate between low and intermediate/high hemodynamic risk was 18% for LEF (sensitivity 80%, specificity 87%, positive predictive value [PPV] 89%, negative predictive value [NPV] 77%, precision 83%) and 0.41 mm/mm Hg for TAPSE/PASP (sensitivity 84%, specificity 81%, PPV 84%, NPV 81%, precision 83%).

Comparing high ($n = 6$) with intermediate hemodynamic risk, a loss of anteroposterior and radial shortening was noted (AEF: 9.5 [8.7–11.9]% vs 17.4 [12.4–22.3]%, $p = 0.010$; REF: 8.2 [6.3–8.8]% vs 16.7 [9.8–23.5]%, $p = 0.024$; Figure 2B). AEF demonstrated excellent ability to discriminate between high and low/intermediate hemodynamic risk; discriminatory power was good for REF and TAPSE/PASP, and lowest (though still significant) for LEF (Figure 3E–H). The optimal cut-off for AEF to discriminate between high and low/intermediate hemodynamic risk was 15% (sensitivity 100%, specificity 83%, PPV 43%, NPV 100%, precision 85%).

Ventricular interdependence and RV and LV volumetry

To demonstrate the evolution of the spatial interventricular relationship during PH-related remodeling, RV and LV

volumetry were compared between distinct levels of RV–PA uncoupling. The results are shown in Figure S5 and are summarized here. RVEF decreased from no or mild uncoupling to intermediate uncoupling ($p = 0.021$), as well as from intermediate to severe uncoupling ($p = 0.044$), with no change in RVSV indexed to BSA (RVSVi; $p = 0.93$ and $p = 0.71$, respectively). RVEDVi and RVESVi both increased from no or mild uncoupling to severe uncoupling ($p = 0.009$ and $p = 0.003$, respectively). RVESVi also increased from no or mild to intermediate uncoupling ($p = 0.039$) with a borderline significant increase ($p = 0.050$) from intermediate to severe uncoupling, whereas the corresponding changes in RVEDVi were not significant ($p = 0.97$ and $p = 0.10$, respectively). In contrast to RV findings, LV ejection fraction (LVEF) was not altered with impairment of RV–PA uncoupling ($p = 0.96$ between no or mild uncoupling and intermediate uncoupling, and $p = 0.07$ between intermediate and severe uncoupling). LV stroke volume index (LVSVi) was impaired with severe compared with intermediate RV–PA uncoupling ($p = 0.005$), but remained stable between no or mild uncoupling and intermediate uncoupling ($p = 0.88$). Consistent with this finding, LV end-diastolic volume index was decreased with severe RV–PA uncoupling ($p = 0.028$ compared with intermediate uncoupling and $p = 0.035$ compared with no or mild uncoupling), whereas LV end-systolic volume index was unchanged ($p = 0.71$ between normal-to-mild and intermediate RV–PA uncoupling, and $p = 0.37$ between intermediate RV–PA uncoupling and severe uncoupling).

Discussion

This study shows that RV contraction patterns change as a function of progressive RV–PA uncoupling and increased hemodynamic-based mortality risk, from decreased longitudinal shortening in patients with low hemodynamic risk and no or mild RV–PA uncoupling, to decreased anteroposterior

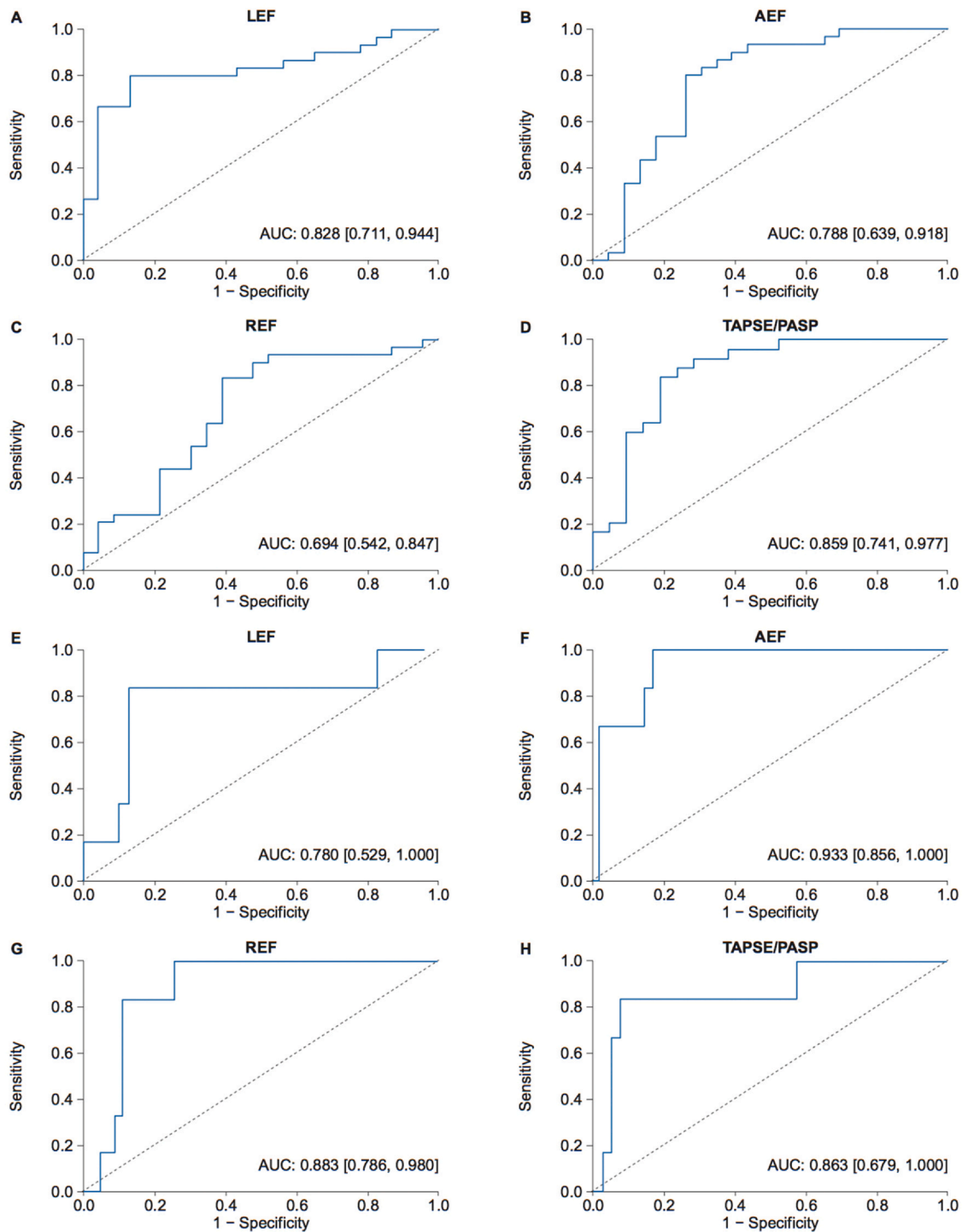


Figure 3 Ability of right ventricular contraction parameters to discriminate risk. Receiver operating characteristic curves show the ability of (A) LEF, (B) AEF, (C) REF, and (D) TAPSE/PASP to discriminate between patients with low hemodynamic risk and those with intermediate/high hemodynamic risk, and the ability of (E) LEF, (F) AEF, (G) REF, and (H) TAPSE/PASP to discriminate between patients with high hemodynamic risk and those with low/intermediate hemodynamic risk, based on the European Society of Cardiology/European Respiratory Society risk stratification scheme.⁹ AUC [95% confidence interval] is shown for each curve. AEF, anteroposterior ejection fraction; AUC, area under the curve; LEF, longitudinal ejection fraction; PASP, pulmonary arterial systolic pressure; REF, radial ejection fraction; TAPSE, tricuspid annular plane systolic excursion.

shortening in patients with severe RV-PA uncoupling, increased RV volumes, decreased LV preload, and advanced hemodynamic mortality risk (Figure 5).

Previous studies have related axial RV shortening to RVEF,^{5,8} hemodynamic parameters (mPAP and cardiac index)⁷

and mortality.^{6,8} The present study is original in relating axial RV shortening also to invasive measurements of Ees/Ea and risk as assessed by invasive hemodynamics. The results confirm the predominant loss of longitudinal shortening in less severe PH and the predominant loss of anteroposterior shortening in

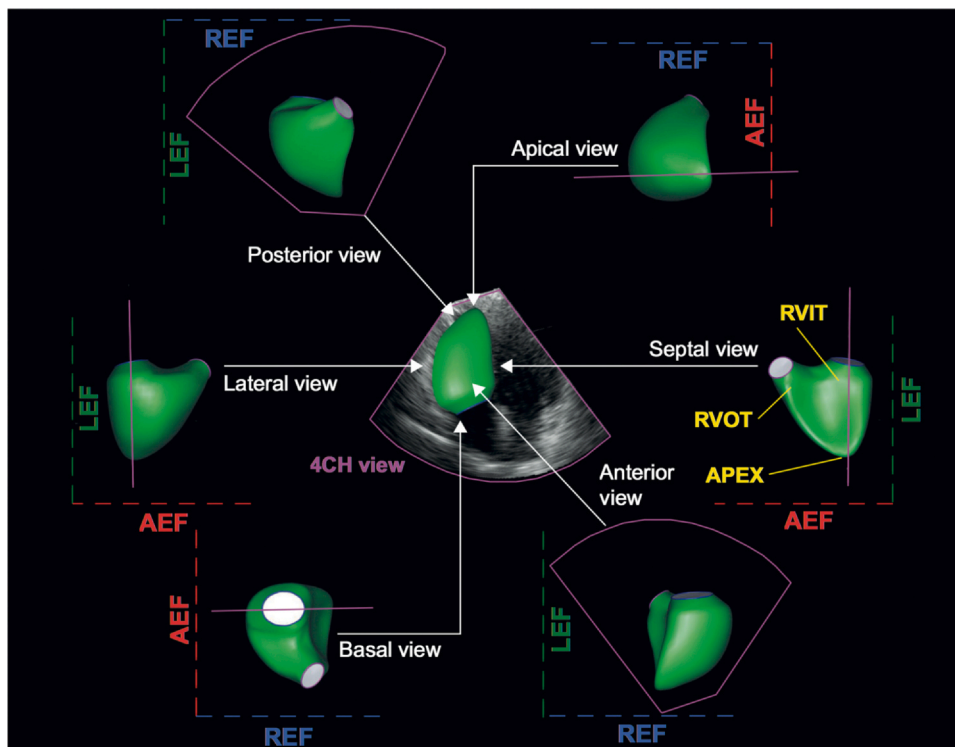


Figure 4 Anatomic shape of the right ventricle. 3D views of the right ventricle of a 61-year-old male patient with hemodynamic exclusion of pulmonary hypertension are shown surrounding a 2D apical 4CH view (positioned in the center with the corresponding RV 3D beutel). For each different 3D view, a pink line indicates the plane of the 2D 4CH view depicted in the center image. Longitudinal (LEF), radial (REF), and anteroposterior (AEF) axes are shown. 2D, two-dimensional; 3D, three-dimensional; 4CH, four-chamber; AEF, anteroposterior ejection fraction; LEF, longitudinal ejection fraction; REF, radial ejection fraction; RVIT, right ventricular inflow tract; RVOT, right ventricular outflow tract.

more advanced PH, and provide additional information on the functional and clinical relevance of RV contraction patterns.

Previous studies suggest a sequence of changes in RV-PA coupling as PH progresses, with initial preservation of Ees/Ea (by adapted increase in Ees) and unchanged RV volumes followed by a late decrease in Ees/Ea and (when Ees/Ea falls below the reserve threshold) RV dilatation, septal shift, and terminal decrease in LV preloading.¹⁻³ While admittedly this sequence of events was not determined in prospectively followed patients, physiological rationale^{1,2} and clinical experience³ allow for the definition of stages of RV-PA uncoupling from normal to heart failure values as were defined in the present study. The results are compatible with previously published work.⁹

The obvious interest in 3D echocardiography is that this bedside technology allows for repetitive measurements of RVEF, which can be considered a relevant surrogate for the Ees/Ea ratio,¹⁶ is a potent predictor of outcome in severe PH,^{17,18} and is now listed in the updated ESC/ERS guidelines.⁹ The further added value of 3D echocardiography, as previously underscored⁸ and shown in the present study, is that it allows analysis of the contribution of regional changes in RV structure and function to ejection. The present data show the high relevance of this approach. 3D echocardiography-based estimation of RV dimensions is known to underestimate RV volumes and stroke volume (index) compared with gold-standard cardiac magnetic resonance imaging.¹⁹ This phenomenon, which is based on the complex

geometry of the right ventricle, is also present in our study and comparable to previously reported differences.

Guidelines for the diagnosis and treatment of PH heavily rely on assessment of mortality risk.⁹ These scores have been derived from clinical experience and rigorous analyses of registries, and have undergone a posteriori validation mainly in PAH. The present study used an adaptation of the score developed by Kylhammar et al,¹⁴ which has recently undergone further validation for prediction of long-term survival in PAH.²⁰ In the present study, only invasive hemodynamics were included for risk stratification. Although other simplified ESC/ERS risk assessments based on mean grades have successfully discriminated prognosis,²¹ this remains a limitation of our risk assessment. Recent studies have validated PAH risk scores for patients with chronic thromboembolic PH.^{22,23} The same scores have not been validated for patients with HFpEF, who formed a small proportion of the present study population, and were included for the purpose of consistency. This may also be considered a limitation.

Longitudinal RV shortening derives from the longitudinally aligned myofibers of the subendocardial layer of the RV myocardium (Figure 1B).²⁴ Radial motion originates from contraction of the circumferentially aligned subepicardial myofibers.¹² LV contraction and septal bowing into the RV lumen result in RV anteroposterior shortening by stretching the RV free wall over the interventricular septum, moving the RV free wall insertion lines towards each other.²⁴

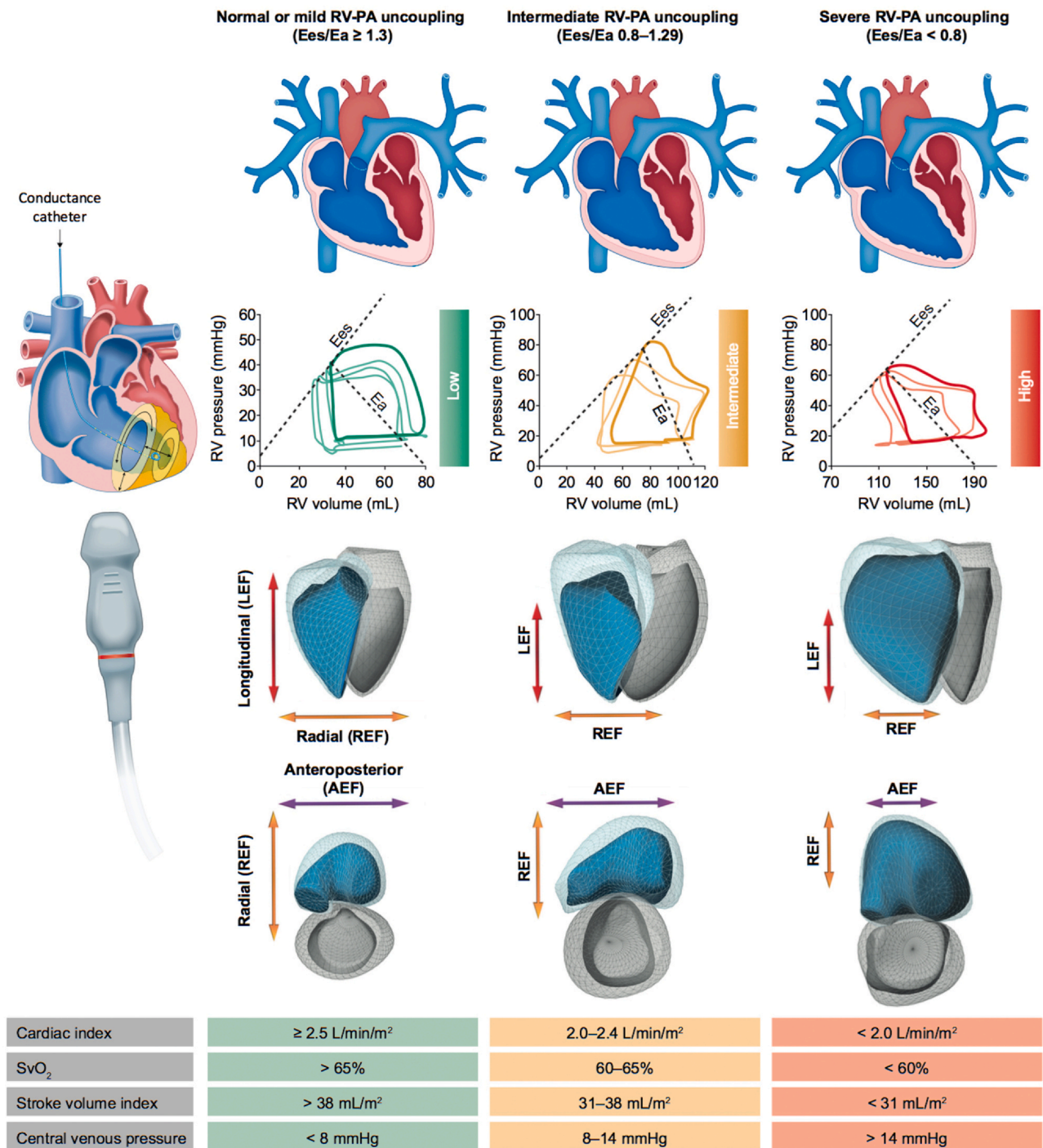


Figure 5 RV contraction patterns at different levels of RV-PA coupling and mortality risk. In a cohort comprising 53 patients with suspected or confirmed pulmonary hypertension, RV contraction patterns showed characteristic alterations at different levels of RV-PA uncoupling and hemodynamic risk. Early RV-PA uncoupling was characterized by reduced RV longitudinal function, whereas advanced RV-PA uncoupling was accompanied by reduced RV anteroposterior shortening. RV-PA coupling was measured from multibeat pressure–volume loops obtained by conductance catheterization with Valsalva-induced reduction of RV preload (example loops are shown alongside a diagram of a correctly positioned conductance catheter). Contraction patterns were measured by three-dimensional echocardiography (example images are shown alongside a sonographic probe). Double arrows indicate the direction of LEF (red), REF (orange), and AEF (purple). Differences in LEF, REF, and AEF across RV-PA uncoupling levels are shown as different arrow lengths. The color-coded table indicates hemodynamic parameters for risk stratification, with thresholds according to the 2022 European Society of Cardiology/European Respiratory Society guidelines.⁹ AEF, anteroposterior ejection fraction; Ea, arterial elastance; Ees, end-systolic elastance; LEF, longitudinal ejection fraction; REF, radial ejection fraction; RV, right ventricular; RV-PA, right ventricular-pulmonary arterial; SvO₂, mixed venous oxygen saturation.

In the present study, 2D echocardiographic parameters reflecting longitudinal function (TAPSE, RVGLS, and RVFWLS) showed a significant decrease from no or mild RV–PA uncoupling to intermediate uncoupling but not from intermediate to severe uncoupling, similar to LEF. Interestingly however, S' , which is also commonly applied in echocardiographic right cardiac longitudinal functional assessment, showed no significant difference between the distinct levels of RV–PA uncoupling.

It is of interest that LVEF was maintained in the presence of severe RV–PA uncoupling, whereas LVSVi was decreased. This is compatible with the notion that RV–PA uncoupling leads to impaired LVSVi through impaired LV preload.² There is however evidence that at later stages of PH than in the present study, negative diastolic ventricular interaction and LV underfilling ultimately lead to depressed LV systolic function.²⁵

This study has several limitations. First, the number of patients included was small. However, sophisticated methodology with combined standard and conductance catheterization, 3D echocardiography, and strain analysis limits recruitment of severely ill patients with PH. With a small sample size, the results may not be representative of the population and may be subject to random variation. The small sample size may also cause a type II error. Therefore, larger, prospective studies are warranted. Second, a simplified version of the ESC/ERS risk stratification scheme without 6-minute walking distance and functional class was used. Third, the ESC/ERS risk stratification scheme has not been validated for patients with HFpEF or individuals without PH. Fourth, the reported data are cross-sectional, which limits the interpretation of measurements as indicators of disease progression. Therefore, longitudinal studies are warranted. Fifth, patients with atrial fibrillation had to be excluded, as the approach is not applicable with varying cardiac cycle length.

In conclusion, our data show that the early phase of RV impairment is characterized by reduced RV longitudinal function, whereas the advanced phase is associated with reduced RV anteroposterior shortening and LV preload. Studies are needed to characterize further the deformational processes leading to mutual impairment of both ventricles in RV–PA uncoupling, and to determine the role of 3D echocardiography in risk stratification in PH.

Author contributions

K.T. and A.K. supervised the project. K.T., A.K., Z.A.R., and A.Y. have substantially contributed to the conception and design of the work. K.T., A.K., Z.A.R., A.Y., S.Y., B.K.L., A.F., M.R., N.C.K., and B.B.R. have performed the acquisition, analysis and/or interpretation of data for the work. All authors participated in the drafting and critical revising of the work for important intellectual content, gave final approval of the version to be published, and agree to be accountable for all aspects of the work in ensuring that

questions related to the accuracy or integrity of any part of the work are appropriately investigated and resolved.

Disclosure statement

This study was funded by Deutsche Forschungsgesellschaft, Grant Agreement Number CRC 1213, Project B08.

Dr Rako, Ms Yildiz, Mr da Rocha, Dr Kremer and Dr Vadász report nonfinancial support from the University of Giessen during the conduct of the study. Dr Yogeswaran reports nonfinancial support from the University of Giessen during the conduct of the study and personal fees from MSD outside the current study. Dr Lakatos, Dr Fábíán, and Dr Kovács report personal fees from Argus Cognitive, Inc. during the conduct of the study. Dr Ghofrani reports nonfinancial support from the University of Giessen and grants from the German Research Foundation during the conduct of the study and personal fees from Bayer, Actelion, Pfizer, Merck, GSK and Takeda, grants and personal fees from Novartis, Bayer HealthCare and Encysive/Pfizer, and grants from Aires, the German Research Foundation, Excellence Cluster Cardiopulmonary Research, and the German Ministry of Education and Research outside the current study. Dr Seeger reports grants from the German Research Foundation and nonfinancial support from the University of Giessen during the conduct of the current study and personal fees from Pfizer and Bayer Pharma AG outside the submitted work. Dr Gall reports grants from the German Research Foundation and nonfinancial support from the University of Giessen during the conduct of the current study and personal fees from Actelion, AstraZeneca, Bayer, BMS, GSK, Janssen-Cilag, Lilly, MSD, Novartis, OMT, Pfizer, and United Therapeutics outside the current study. Dr Richter reports nonfinancial support from the University of Giessen during the conduct of the current study and research support from United Therapeutics and Bayer, speaker honoraria from Bayer, Actelion, Mundipharma, Roche, and OMT, and consultancy fees from Bayer outside the submitted work. Dr Bauer reports consultancy fees from Bristol Myers Squibb/Pfizer and speaker fees from Bristol Myers Squibb/Pfizer, AstraZeneca and Amgen. Dr Tedford reports no direct conflicts of interest during the conduct of the current study and consulting relationships with Abiomed (research advisory board), Medtronic, Abbott (steering committee), Aria CV Inc., Acceleron/Merck (steering committee and hemodynamic core lab work for Merck), Alleviant, CareDx, Cytokinetics, Itamar, Edwards LifeSciences (national principal investigator for the RIGHT-FLOW clinical trial), Eidos Therapeutics, Lexicon Pharmaceuticals, and Gradient outside the submitted work. Dr Naeije reports relationships including consultancies, speaker's fees and membership of advisory boards with AOP Orphan Pharmaceuticals, Johnson & Johnson, Lung Biotechnology Corporation and United Therapeutics. Dr Tello reports nonfinancial support from the University of Giessen during the conduct of the current study and speaker

honoraria from Actelion and Bayer outside the submitted work.

We thank Claire Mulligan, PhD (Beacon Medical Communications Ltd, Brighton, UK) for editorial assistance, funded by the University of Giessen.

Appendix A. Supporting information

Supplementary data associated with this article can be found in the online version at [doi:10.1016/j.healun.2023.07.004](https://doi.org/10.1016/j.healun.2023.07.004).

References

1. Vonk Noordegraaf A, Chin KM, Haddad F, et al. Pathophysiology of the right ventricle and of the pulmonary circulation in pulmonary hypertension: an update. *Eur Respir J* 2019;53:1801900.
2. Sanz J, Sanchez-Quintana D, Bossone E, Bogaard HJ, Anatomy Naeije R. Function, and dysfunction of the right ventricle: JACC state-of-the-art review. *J Am Coll Cardiol* 2019;73:1463-82.
3. Tello K, Dalmer A, Axmann J, et al. Reserve of right ventricular-arterial coupling in the setting of chronic overload. *Circ Heart Fail* 2019;12:e005512.
4. Brown SB, Raina A, Katz D, Szerlip M, Wieggers SE, Forfia PR. Longitudinal shortening accounts for the majority of right ventricular contraction and improves after pulmonary vasodilator therapy in normal subjects and patients with pulmonary arterial hypertension. *Chest* 2011;140:27-33.
5. Kind T, Mauritz GJ, Marcus JT, van de Veerdonk M, Westerhof N, Vonk-Noordegraaf A. Right ventricular ejection fraction is better reflected by transverse rather than longitudinal wall motion in pulmonary hypertension. *J Cardiovasc Magn Reson* 2010;12:35.
6. Mauritz GJ, Kind T, Marcus JT, et al. Progressive changes in right ventricular geometric shortening and long-term survival in pulmonary arterial hypertension. *Chest* 2012;141:935-43.
7. Pica S, Ghio S, Tonti G, et al. Analyses of longitudinal and of transverse right ventricular function provide different clinical information in patients with pulmonary hypertension. *Ultrasound Med Biol* 2014;40:1096-103.
8. Smith BC, Dobson G, Dawson D, Charalampopoulos A, Grapsa J, Nihoyannopoulos P. Three-dimensional speckle tracking of the right ventricle: toward optimal quantification of right ventricular dysfunction in pulmonary hypertension. *J Am Coll Cardiol* 2014;64:41-51.
9. Humbert M, Kovacs G, Hoeper MM, et al. 2022 ESC/ERS guidelines for the diagnosis and treatment of pulmonary hypertension. *Eur Heart J* 2022;43:3618-731.
10. Lang RM, Badano LP, Mor-Avi V, et al. Recommendations for cardiac chamber quantification by echocardiography in adults: an update from the American Society of Echocardiography and the European Association of Cardiovascular Imaging. *J Am Soc Echocardiogr* 2015;28:1-39 e14.
11. Tokodi M, Staub L, Budai A, et al. Partitioning the right ventricle into 15 segments and decomposing its motion using 3D echocardiography-based models: the updated ReVISION method. *Front Cardiovasc Med* 2021;8:622118.
12. Lakatos B, Toser Z, Tokodi M, et al. Quantification of the relative contribution of the different right ventricular wall motion components to right ventricular ejection fraction: the ReVISION method. *Cardiovasc Ultrasound* 2017;15:8.
13. Ireland CG, Damico RL, Kolb TM, et al. Exercise right ventricular ejection fraction predicts right ventricular contractile reserve. *J Heart Lung Transplant* 2021;40:504-12.
14. Kylhammar D, Kjellstrom B, Hjalmarsson C, et al. A comprehensive risk stratification at early follow-up determines prognosis in pulmonary arterial hypertension. *Eur Heart J* 2018;39:4175-81.
15. Gall H, Yogeswaran A, Fuge J, et al. Validity of echocardiographic tricuspid regurgitation gradient to screen for new definition of pulmonary hypertension. *EclinicalMedicine* 2021;34:100822.
16. Naeije R, Richter MJ, Rubin LJ. The physiological basis of pulmonary arterial hypertension. *Eur Respir J* 2022;59:2102334.
17. Lewis RA, Johns CS, Cogliano M, et al. Identification of cardiac magnetic resonance imaging thresholds for risk stratification in pulmonary arterial hypertension. *Am J Respir Crit Care Med* 2020;201:458-68.
18. Alabed S, Shahin Y, Garg P, et al. Cardiac-MRI predicts clinical worsening and mortality in pulmonary arterial hypertension: a systematic review and meta-analysis. *JACC Cardiovasc Imaging* 2021;14:931-42.
19. Shimada YJ, Shiota M, Siegel RJ, Shiota T. Accuracy of right ventricular volumes and function determined by three-dimensional echocardiography in comparison with magnetic resonance imaging: a meta-analysis study. *J Am Soc Echocardiogr* 2010;23:943-53.
20. Kylhammar D, Hjalmarsson C, Hesselstrand R, et al. Predicting mortality during long-term follow-up in pulmonary arterial hypertension. *ERJ Open Res* 2021;7:00837-2020.
21. Sanna L, Todea A. Risk assessment tools for survival prognosis: An era of new surrogacy endpoints for clinical outcome measurement in pulmonary arterial hypertension clinical trials? *Respir Med Res* 2022;81:100893.
22. Delcroix M, Staehler G, Gall H, et al. Risk assessment in medically treated chronic thromboembolic pulmonary hypertension patients. *Eur Respir J* 2018;52:1800248.
23. Sandqvist A, Kylhammar D, Bartfay SE, et al. Risk stratification in chronic thromboembolic pulmonary hypertension predicts survival. *Scand Cardiovasc J* 2021;55:43-9.
24. Kovacs A, Lakatos B, Tokodi M, Merkely B. Right ventricular mechanical pattern in health and disease: beyond longitudinal shortening. *Heart Fail Rev* 2019;24:511-20.
25. Naeije R, Badagliacca R. The overloaded right heart and ventricular interdependence. *Cardiovasc Res* 2017;113:1474-85.